

Theoretical Study of Magnetism and Superconductivity in 3d Transition -Metal-M gB₂ Alloys

Prabhakar P. Singh and P. Jiji Thomas Joseph

Department of Physics, Indian Institute of Technology, Powai, Mumbai- 400076, India

Abstract

We have studied the electronic structure of 3d transition-metal-M gB₂ alloys, M g_{0.97}TM_{0.03}B₂, (TM = Sc; Ti; V; Cr; Mn; Fe; Co; Ni; Cu; Zn) using Korringa-Kohn-Rostoker coherent-potential approximation (KKR-CPA) method in the atomic-sphere approximation (ASA). For *unpolarized* calculations, our results for M g_{0.97}TM_{0.03}B₂ alloys are similar to that of 3d impurities in other s and s-p metals. In particular, the local densities of states (DOS) associated with the 3d impurities are similar to our earlier work on 3d impurities in bulk Al [P. P. Singh, Phys. Rev. B **43**, 3975 (1991), P. P. Singh, J. Phys.: Condens. Matter **3**, 3285 (1991)]. For *spin-polarized* calculations, we find only the alloys of V; Cr; Mn; Fe and Co with M gB₂ to be magnetic of all the 3d elements. We also find that Cr and Mn in M gB₂ have a relatively large local magnetic moment of 2.43 μ_B and 2.87 μ_B , respectively. We have used the *unpolarized*, self-consistent potentials of M g_{0.97}TM_{0.03}B₂ alloys, obtained within the coherent-potential approximation, to calculate the electron-phonon coupling constant using the Gaspari-Georff formalism and the superconducting transition temperature T_c using the Allen-Dynes equation. We find that the calculated T_c is the lowest for M g_{0.97}Cr_{0.03}B₂ and the highest for M g_{0.97}Zn_{0.03}B₂, in qualitative agreement with experiment. The calculated trend in variation of T_c from Mn to Zn is also similar to the available experimental data. Our analysis of the variation in T_c, in terms of the DOS and the spectral function along to A direction, shows the variation to be an interplay between the total DOS at the Fermi energy and the creation/removal of states along to A direction [P. P. Singh, cond-mat/0201093].

PACS numbers: 74.25.Jb, 74.70.Ad

I. Introduction

The nature of interaction responsible for superconductivity in $M\text{-}gB_2$ [1, 2, 3, 4, 5, 6, 7, 8, 9, 10, 11, 12, 13, 14, 15, 16] suggests a gradual decrease in the superconducting transition temperature, T_c , upon addition of impurities [17, 18, 19, 20] with increasing *electron/atom* ratio. A systematic increase in the number of available electrons is expected to fill up the holes in $M\text{-}gB_2$, which are coupled strongly to the in-plane bond-stretching mode of B, and thereby reduce the strength of the electron-phonon coupling resulting in a decrease in T_c . The observed variation in T_c of alloys of Al with $M\text{-}gB_2$ and its understanding in terms of a gradual filling up of holes provides a good example of this picture [21, 22].

Since the *electron/atom* ratio increases as one goes from Sc to Zn; based upon the above argument one expects the T_c to systematically decrease as the different elements from the 3d row are added to $M\text{-}gB_2$. However, the experimentally observed changes in T_c of 3d transition-metal- $M\text{-}gB_2$ alloys [20] do not seem to follow the expected trend of a systematic decrease in T_c as one goes from Sc to Zn. For example, a 3% Mn-doped $M\text{-}gB_2$ ($Mg_{0.97}Mn_{0.03}B_2$) has a T_c of only 33.1 K; while $M\text{-}gB_2$ doped similarly with Fe, Co and Ni show T_c 's of 37.8, 35.7 and 37.8 K; respectively [20]. Surprisingly, Zn-doped $M\text{-}gB_2$ shows the highest T_c ($= 38.4\text{ K}$) of all the transition-metal- $M\text{-}gB_2$ alloys investigated so far [19, 20]. The observed changes in T_c of transition-metal-doped $M\text{-}gB_2$ alloys, especially as one goes from Fe to Zn; are unexpected even after making allowances for magnetic effects [23, 24].

To understand the changes in the electronic structure and the superconducting properties of $M\text{-}gB_2$ alloys upon addition of 3d transition-metal impurities, we have carried out *ab initio* studies of $Mg_{0.97}TM_{0.03}B_2$ ($TM = \text{Sc; Ti; V; Cr; Mn; Fe; Co; Ni; Cu; Zn}$) alloys using density-functional-based methods. We have used Korringa-Kohn-Rostoker coherent-potential approximation method [25] in the atomic-sphere approximation (KKR-ASA CPA) [26] for taking into account the effects of disorder, Gaspari-Gyorffy formalism [27] for calculating the electron-phonon coupling constant λ , and Allen-Dynes equation [23, 24] for calculating T_c in $Mg_{0.97}TM_{0.03}B_2$ alloys. For understanding the variation in T_c as one goes from Sc to Zn, we have analyzed our results in terms of the changes in the spectral function [25] along to A [21, 28] and the densities of states (DOS), in particular, the changes in the B p and the transition-metal d contributions to the total DOS. The changes in the magnetic alloys are described in terms of spin-resolved densities of states and the local magnetic mo-

ments. Before we describe our results, we outline some of the computational details of our calculation.

II. Computational Details

The charge self-consistent electronic structure of unpolarized as well as spin-polarized $M_{0.97}TM_{0.03}B_2$ alloys has been calculated using the KKR-ASA CPA method. We have used the CPA successfully to describe the electronic structure of Al doped MgB_2 alloys [21]. We parametrized the exchange-correlation potential as suggested by Perdew-Wang within the generalized gradient approximation [29]. The Brillouin zone (BZ) integration was carried out using 1215 \mathbf{k} -points in the irreducible part of the BZ. For DOS calculations, we added a small imaginary component of 1 mRy to the energy and used 4900 \mathbf{k} -points in the irreducible part of the BZ. The lattice constants for $M_{0.97}TM_{0.03}B_2$ were fixed at the MgB_2 values. The Wigner-Seitz radius for Mg was slightly larger than that of B , while the Wigner-Seitz radii of the impurities were equal to their bulk value as given in Ref. [30]. The maximum l used was $l_{max} = 3$.

As indicated above, the electron-phonon coupling constant was calculated using Gaspari-Gyorffy formalism with the charge self-consistent potentials of unpolarized $M_{0.97}TM_{0.03}B_2$ alloys obtained with the KKR-ASA CPA method. Subsequently, the variation of T_c was calculated using Allen-Dynes equation. The average value of phonon frequency ω_{ln} for MgB_2 was taken from Ref. [9] and $\lambda = 0.09$.

III. Results and Discussion

In this section we present the results of our self-consistent electronic structure calculations for $M_{0.97}TM_{0.03}B_2$ alloys. We first describe the results of the *unpolarized* calculations in terms of the total and the sub-lattice resolved DOS, including the local DOS due to the 3d transition-metal impurity. From our *spin-polarized* calculations, described next, we find only the alloys of $V; Cr; Mn; Fe$ and Co with MgB_2 to be magnetic of all the 3d elements. These results are discussed using the spin-resolved DOS and the local moments. Finally, the calculated variation in T_c for $M_{0.97}TM_{0.03}B_2$ alloys is compared with the available experimental data, and analyzed in terms of the DOS and the spectral function along to

A.

A. Unpolarized Total and Local Densities of States

In Fig. 1 we show the calculated densities of states of $\text{M}_{0.97}\text{TM}_{0.03}\text{B}_2$ alloys from Sc to Zn, including the total DOS, $N(E)$; and the concentration-weighted, sub-lattice resolved DOS for the two inequivalent sub-lattices ($N^{\text{sub}}(E)$) in $\text{M}_{0.97}\text{B}_2$. The two inequivalent sub-lattices consist of the M g and the transition-metal on one sub-lattice ($N_1^{\text{sub}}(E) = 0.97N_{\text{M g}}^{\text{sub}}(E) + 0.03N_{\text{TM}}^{\text{sub}}(E)$) and B on the other two sub-lattices ($N_2^{\text{sub}}(E) = 2N_{\text{B}}^{\text{sub}}(E)$). As we go from Sc to Zn, the increase in the *electron/atom* ratio moves the Fermi energy, E_F , as well as increases the hybridization of the host s-p bands with the impurity d-band. The change in E_F has important consequences for the superconducting properties of these alloys, as discussed later. The inward movement of the d-band as we go from Sc to Zn is clearly manifested in the total DOS as well as the concentration-weighted DOS of M g sub-lattice. However, we find that the DOS at the B sub-lattice remains largely unaffected due to the transition-metal impurity, although the movement of E_F changes the B contribution to the total DOS at E_F .

To be able to examine the changes in the DOS of the transition-metal impurities and to show the movement of the d-band as we go from Sc to Zn, we show in Fig. 2 the DOS of the transition metal impurity $N_{\text{TM}}^{\text{sub}}(E)$ on the M g sub-lattice in $\text{M}_{0.97}\text{TM}_{0.03}\text{B}_2$ alloys. We find that the d-level crosses E_F between Cr and Mn, resulting in a very high density of states at E_F for these alloys. The relatively high DOS for $N_{\text{Cr}}^{\text{sub}}(E_F)$ and $N_{\text{Mn}}^{\text{sub}}(E_F)$ points to the possibility of local magnetic moment formation at the impurity sites. By the time we come to Zn impurity, the d-level is well inside E_F and the impurity contribution to the total DOS has reduced significantly. We also find that the lowering of d-level with increasing d-electrons is accompanied by the narrowing of the d-band. For example, in the case of Zn impurity the width of the d-band is the narrowest, indicating almost an atomic-like behavior of these d-electrons. It is interesting to note that these results are qualitatively similar to our results on 3d transition-metal impurities in Al [31, 32]

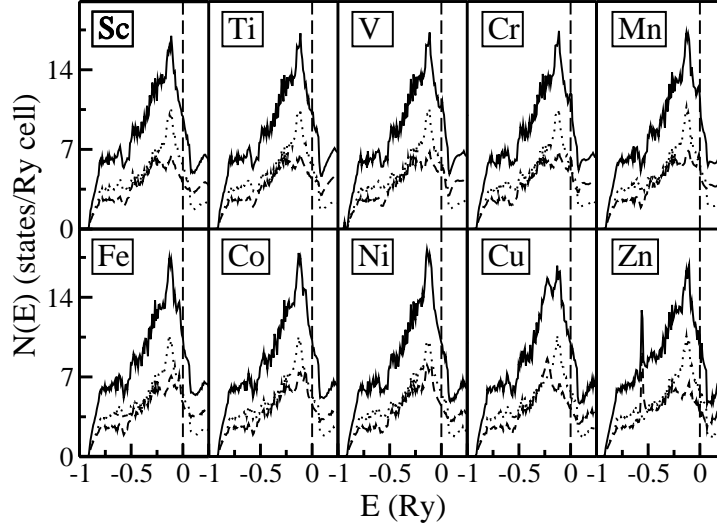


FIG. 1: The calculated total density of states (solid line) for $M_{90.97}TM_{0.03}B_2$ alloys. The contributions to the total DOS from the M_{g} sub-lattice (dashed line) and the B sub-lattice (dotted line) are also shown. Note that the M_{g} sub-lattice contains both M_{g} and the transition-metal (TM) impurity atoms. The vertical dashed line indicates the Fermi energy.

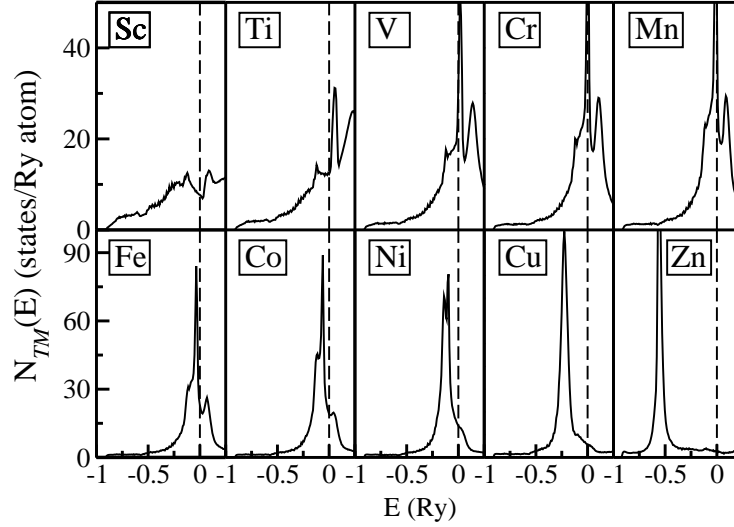


FIG. 2: The calculated total local density of states (solid line) for transition-metal impurity in $M_{90.97}TM_{0.03}B_2$ alloys. The vertical dashed line indicates the Fermi energy.

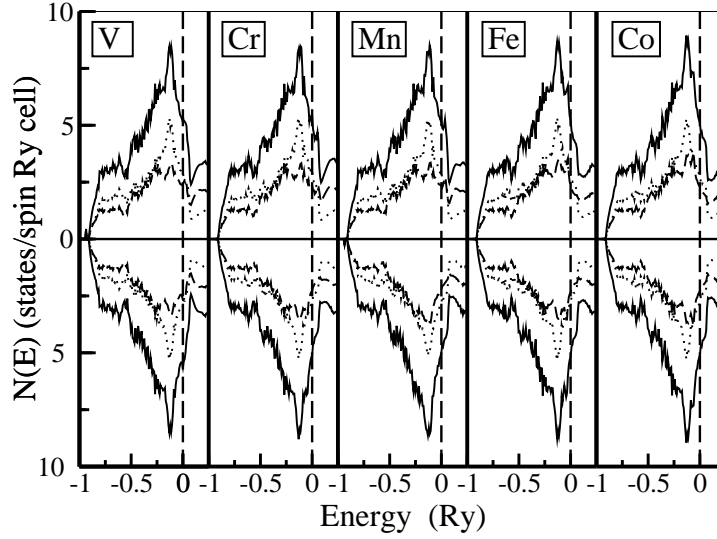


FIG. 3: The calculated total density of states (solid line) for $M_{0.97}TM_{0.03}B_2$ alloys with majority (upper panel) and minority spins (lower panel). The majority and minority spins contributions to the total DOS from the $M_{0.97}$ sub-lattice (dashed line) and the $B_{0.03}$ sub-lattice (dotted line) are shown in their respective panels. The vertical dashed line indicates the Fermi energy.

B. Spin-Polarized Total and Local Densities of States

The results of our spin-polarized calculations for $M_{0.97}TM_{0.03}B_2$ alloys are shown in Figs. 3-5. Our calculations show that the alloys of $V_{0.97}Cr_{0.03}B_2$, $Mn_{0.97}Fe_{0.03}B_2$ and $Co_{0.97}B_2$ are exchange-split, as can be seen in Fig. 3 where we have plotted the spin-polarized total and the concentration-weighted, sub-lattice resolved DOS for $V_{0.97}Cr_{0.03}B_2$, $Mn_{0.97}Fe_{0.03}B_2$ and $Co_{0.97}B_2$. Once again, we find that the $B_{0.03}$ sub-lattice remains unaffected due to magnetic moment formation at the impurity site on the $M_{0.97}$ sub-lattice. To clearly show the changes in the majority and the minority spin DOS of the $M_{0.97}$ sub-lattice due to exchange-splitting in the DOS of the impurity atom, we show in Fig. 4 the spin-resolved total DOS due to the impurity atom. As expected from the unpolarized calculations, the exchange splitting is the largest for $Cr_{0.03}$ and $Mn_{0.03}$ alloys. The exchange-splitting in the DOS due to the impurity atom leads to local moment formation at these sites with $Cr_{0.03}$ and $Mn_{0.03}$ having local moments of $2.43 \mu_B$ and $2.37 \mu_B$, respectively. The local moment on $Co_{0.03}$ is very small ($0.01 \mu_B$). Note that the total DOS of the impurity is dominated by the d contribution and the local moments arise almost entirely due to the impurity d electrons.

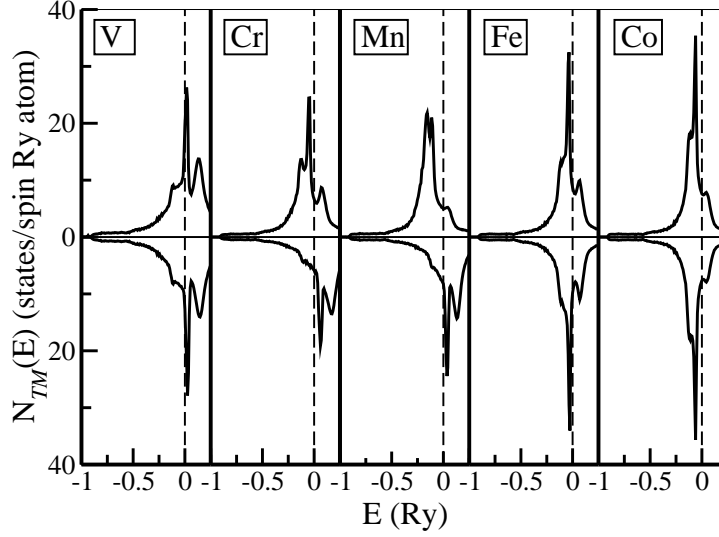


FIG. 4: The calculated total local density of states (solid line) for transition-metal impurity in $\text{Mg}_{0.97}\text{TM}_{0.03}\text{B}_2$ alloys with majority (upper panel) and minority spins (lower panel). The vertical dashed line indicates the Fermi energy.

It must be pointed out that the calculation of local moments in alloys is sensitive to the volume that one associates with the impurity atom. Given the availability of electrons around the Mg sub-lattice in MgB_2 alloys, a judicious choice of the impurity-atom volume is essential for a reliable description of the local moments. In our calculations, we have chosen the impurity atomic volume to be equal to the observed bulk value as given in Ref. [30]. However, it is clear that Cr and Mn will show large local moments in MgB_2 .

C. Superconducting Transition Temperature

We have studied the electronic structure of $\text{Mg}_{0.97}\text{TM}_{0.03}\text{B}_2$ alloys as a prelude to understanding the superconducting properties, especially the superconducting transition temperature T_c , of these alloys. In Fig. 6 we show our calculated T_c as well as the observed T_c [19, 20] for $\text{Mg}_{0.97}\text{TM}_{0.03}\text{B}_2$ alloys. The calculated variation in T_c across the 3d row is similar to the one observed experimentally for Mn to Zn in MgB_2 [19, 20]. Note that our calculated T_c for MgB_2 is equal to $\sim 30\text{K}$, which is consistent with the results of other works [7, 9, 10] with similar approximations.

The total DOS and the spectral function along Γ to A at E_F are expected to play an im-

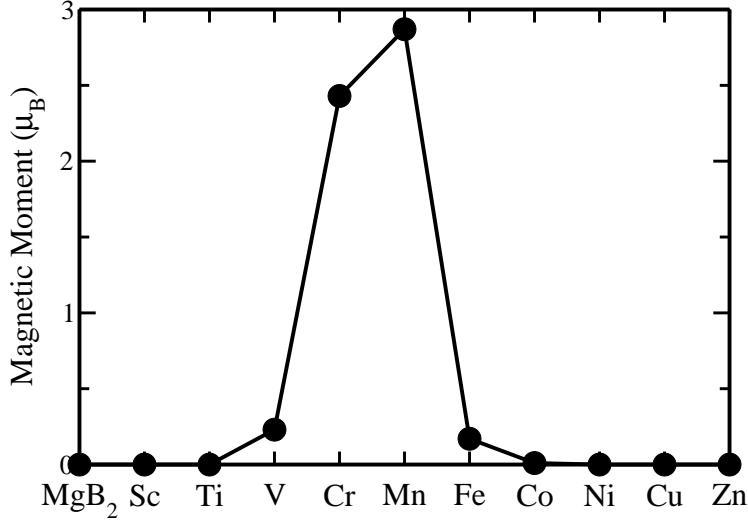


FIG. 5: The calculated local magnetic moment (filled circle) of the transition-metal impurity in $M_{90:97}TM_{0:03}B_2$ alloys.

portant role in deciding the T_c of $M_{90:97}TM_{0:03}B_2$ alloys. Thus, in the following we examine the changes in these two quantities in $M_{90:97}TM_{0:03}B_2$ alloys as we go from Sc to Zn. In Fig. 7 we show the total DOS, $N(E_F)$, the B p contribution to $N_B^{sub}(E_F)$ and the impurity d contribution to $N_{TM}^{sub}(E_F)$ at the Fermi energy. Our calculations show $M_{90:97}Cr_{0:03}B_2$ to have the lowest T_c of all the 3d alloys, which coincides with the highest $N(E_F)$ of $11.93 \text{ states/RY cell}$ as well as the highest d contribution to the $N_{CF}^{sub}(E_F)$ of $66.15 \text{ states/RY atom}$, as can be seen in Fig. 7. In contrast, the B p contribution is not enhanced resulting in the lowest T_c for $M_{90:97}Cr_{0:03}B_2$ within our approach. Similarly, the T_c for $M_{90:97}Mn_{0:03}B_2$ is also small in comparison with other alloys. Here, we like to point out that the exchange-splitting will reduce $N_{TM}^{sub}(E_F)$, leading to a smaller $N(E_F)$ in the case of magnetic alloys. Thus, within our approach, it would have led to an increase in T_c . However, the inclusion of magnetism with its pair-breaking effects [23, 24] will further reduce the T_c . The gradual increase in T_c from Mn to Zn is due to enhanced B p contribution to $N_B^{sub}(E_F)$ as well as a substantial decrease in the impurity d contribution to $N_{TM}^{sub}(E_F)$ as shown in Fig. 7.

To further clarify the reasons for the changes in T_c in $M_{90:97}TM_{0:03}B_2$ alloys, as we go from Sc to Zn, we show in Fig. 8(a)-(d) the spectral function, $A(\mathbf{k}, E_F)$, calculated along to A direction in $M_{90:97}TM_{0:03}B_2$ alloys. For comparison we have also plotted $A(\mathbf{k}, E_F)$ for

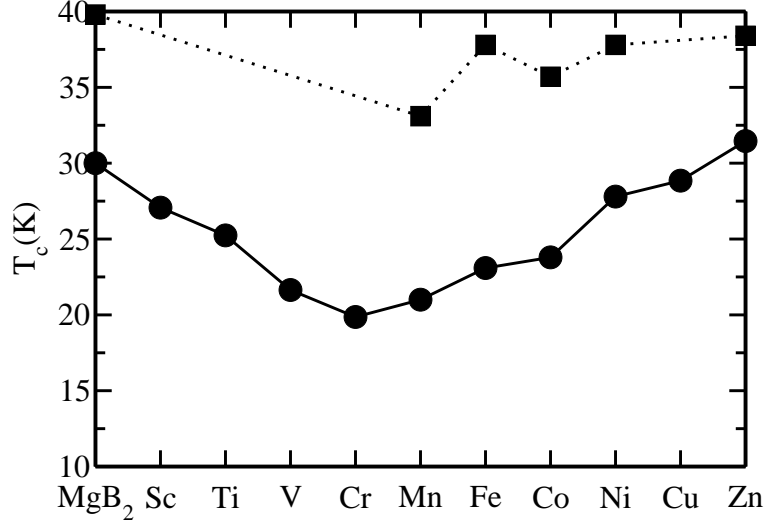


FIG. 6: The calculated (filled circle) and the experimental (filled square) variation of T_c in $M_{90:97}TM_{0:03}B_2$ alloys.

$M_{90:97}B_2$ in Figs. 8(a) and (d). As described in Ref. [21], the additional states created along to A direction reduce the coupling between the hole-like cylindrical Fermi sheets with the phonons which, in turn, reduces the T_c . Thus an alloy with A (\mathbf{k}, E_F) similar to that of $M_{90:97}B_2$ will show a T_c close to that of $M_{90:97}B_2$. Carrying out such a comparison in Fig. 8, we find that $M_{90:97}Zn_{0:03}B_2$ will have a T_c close to that of $M_{90:97}B_2$, while $M_{90:97}V_{0:03}B_2$ will show the lowest T_c of them all. The fact that our calculation shows $M_{90:97}Cr_{0:03}B_2$ to have a lower T_c than $M_{90:97}V_{0:03}B_2$ is due to the relatively high impurity DOS at E_F . In addition, in the case of Cr and Mn impurity in $M_{90:97}B_2$, the magnetic effects will further reduce the T_c [24]. These results reinforce the observation made in Ref. [21] that the way T_c changes in $M_{90:97}B_2$ upon alloying depends dramatically on the location of the added/modified \mathbf{k} -resolved states on the Fermi surface.

IV. Summary

We have studied the electronic structure of 3d transition-metal- $M_{90:97}B_2$ alloys using Korringa-Kohn-Rostoker coherent-potential approximation method in the atomic-sphere approximation. Our results for the *unpolarized* calculations are similar to that of 3d impurities in other s and s-p metals. From *spin-polarized* calculations we find that only alloys of

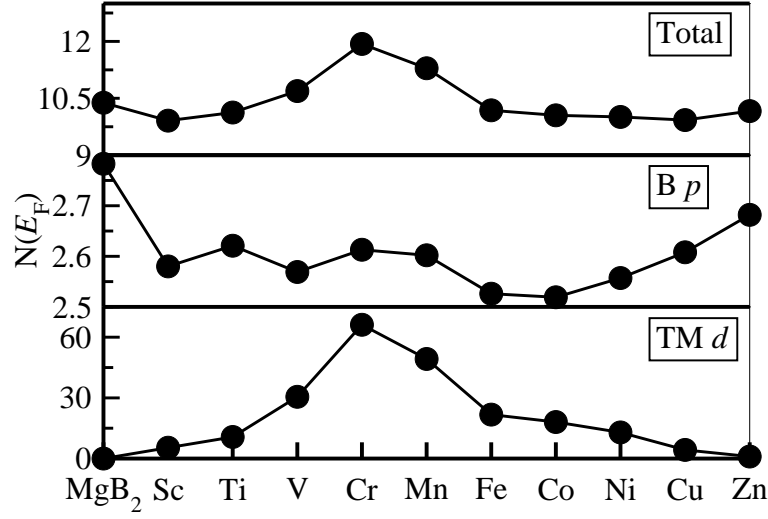


FIG. 7: The calculated total density of states at the Fermi energy (filled circle, upper panel), B p contribution (filled circle, middle panel) and the transition-metal (TM) d contribution (filled circle, lower panel) to the total DOS in $M_{90:97}TM_{0:03}B_2$ alloys.

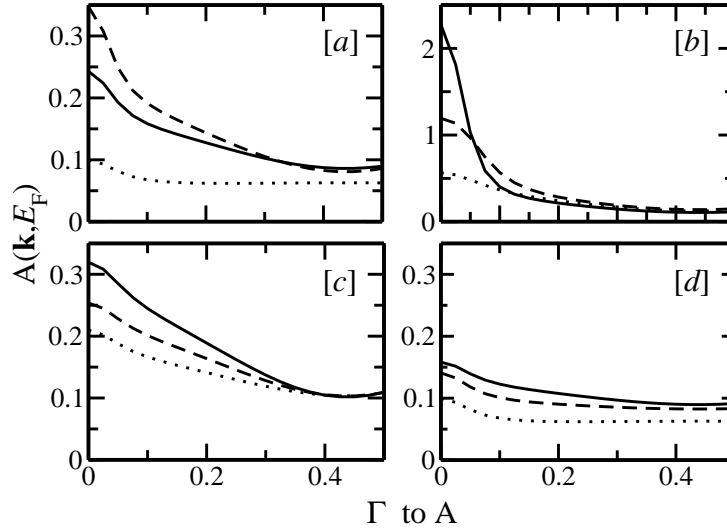


FIG. 8: The calculated spectral function along Γ to A, evaluated at the Fermi energy in $M_{90:97}TM_{0:03}B_2$ alloys. In figures (a)-(d) the solid, dashed and dotted lines correspond to (a) Sc; Ti and MgB₂, (b) V; Cr and Mn, (c) Fe; Co and Ni, and (d) Cu; Zn and MgB₂ alloys, respectively. Note the change in the vertical scale in (b).

V; Cr; Mn; Fe and Co in MgB_2 are magnetic, with Cr and Mn having the largest local magnetic moment of $2.43 \mu_B$ and $2.37 \mu_B$, respectively. We have used the *unpolarized*, self-consistent potentials of $\text{Mg}_{0.97}\text{TM}_{0.03}\text{B}_2$ alloys, obtained within the coherent-potential approximation, to calculate the electron-phonon coupling constant using the Gaspari-Georff formalism. Then, with the help of Allen-Dynes equation we have calculated the superconducting transition temperature T_c of these alloys. We find that the calculated T_c is the lowest for $\text{Mg}_{0.97}\text{Cr}_{0.03}\text{B}_2$ and the highest for $\text{Mg}_{0.97}\text{Zn}_{0.03}\text{B}_2$, in qualitative agreement with experiment. The trend in variation of T_c from Mn to Zn is also similar to the available experimental data.

-
- [1] J. Nagamatsu, N. Nakagawa, T. Muranaka, Y. Zenitani, and J. Akimitsu, *Nature*, **410**, 63 (2001).
 - [2] S. L. Bud'ko, G. Lapertot, C. Petrovic, C. E. Cunningham, N. Anderson, and P. C. Canfield, *Phys. Rev. Lett.* **86**, 1877 (2001).
 - [3] D. G. Hinks and J. D. Jorgensen, *Nature* **411**, 457 (2001).
 - [4] T. Takahashi, T. Sato, S. Souma, T. Muranaka, and J. Akimitsu, *Phys. Rev. Lett.* **86**, 4915 (2001).
 - [5] Cristina Buzea and Tsutomu Yamashita, cond-mat/ 0108265; and references therein.
 - [6] T. Yildirim, O. Gulseren, J. W. Lynn, C. M. Brown, T. J. Udovic, Q. Huang, N. Rogado, K. A. Regan, M. A. Hayward, J. S. Slusky, T. He, M. K. Haas, P. Khalifah, K. Inimaru, and R. J. Cava, *Phys. Rev. Lett.* **86**, 5771 (2001).
 - [7] J. Kortus, I. I. Mazin, K. D. Belashchenko, V. P. Antropov, and L. L. Boyer, *Phys. Rev. Lett.* **86**, 4656 (2001).
 - [8] M. An and W. E. Pickett, *Phys. Rev. Lett.* **86**, 4366 (2001).
 - [9] Y. Kong, O. V. Dolgov, O. Jepsen, and O. K. Andersen, *Phys. Rev. B* **64**, 020501 (2001).
 - [10] K.-P. Bohnen, R. Heid, and B. Renker, *Phys. Rev. Lett.* **86**, 5771 (2001).
 - [11] Prabhakar P. Singh, *Phys. Rev. Lett.* **87**, 087004 (2001).
 - [12] N. I. Medvedeva, A. L. Ivanovskii, J. E. Medvedeva, and A. J. Freeman, *Phys. Rev. B* **64**, 020502 (2001).
 - [13] G. Satta, G. Profeta, F. Bernardini, A. Continenza, and S. Massidda, *Phys. Rev. B* **64**, 104507

- (2001).
- [14] K. D. Belaschenko, M. van Schilfgaarde, and V. P. Antropov, Phys. Rev. B **64**, 092503 (2001).
 - [15] A. Y. Liu, I. I. Mazin, and J. Kortus, Phys. Rev. Lett. **87**, 87005 (2001).
 - [16] H. J. Choi, D. Roundy, H. Sun, M. L. Cohen, and S. G. Louie, cond-mat/0111182 and cond-mat/0111183 (2001).
 - [17] J. Y. Xiang, D. N. Zheng, J. Q. Li, L. Li, P. L. Lang, H. Chen, C. Dong, G. C. Che, Z. A. Ren, H. H. Qi, H. Y. Tian, Y. M. Ni, and X. Z. Zhao, cond-mat/0104366 (2001).
 - [18] Y. G. Zhao, X. P. Zhang, P. T. Qiao, H. T. Zhang, S. L. Jia, B. S. Cao, M. H. Zhu, Z. H. Han, X. L. Wang, and B. L. Gu, Phys. C **361**, 91 (2001).
 - [19] S. M. Kazakov, M. Angst, and J. Karpinski, cond-mat/0103350 (2001).
 - [20] Y. Moritomo and S. Xu, cond-mat/0104568 (2001).
 - [21] Prabhakar P. Singh, cond-mat/0201093 (2002).
 - [22] S. V. Barabash and D. Stroud, cond-mat/0111392 (2001).
 - [23] P. B. Allen and R. C. Dynes, Phys. Rev. B **12**, 905 (1975).
 - [24] P. B. Allen and B. Mitrovic, in *Solid State Physics*, edited by H. Ehrenreich, F. Seitz, and D. Turnbull (Academic, New York 1982), Vol. 37, p. 1.
 - [25] J. S. Faulkner, Prog. Mat. Sci **27**, 1 (1982); and references therein.
 - [26] Prabhakar P. Singh and A. Gonis, Phys. Rev. B **49**, 1642 (1994).
 - [27] G. D. Gaspari and B. L. Gyorffy, Phys. Rev. Lett. **28**, 801 (1972).
 - [28] Prabhakar P. Singh, cond-mat/0201126 (2002).
 - [29] J. P. Perdew and Y. Wang, Phys. Rev. B **45**, 13244 (1992); J. P. Perdew, K. Burke, and M. Ernzerhof, Phys. Rev. Lett. **77**, 3865 (1996).
 - [30] H. L. Skriver, *The LMTO Method* (Springer-Verlag, Berlin, 1984).
 - [31] Prabhakar P. Singh, Phys. Rev. B **43**, 3975 (1991).
 - [32] Prabhakar P. Singh, J. Phys.: Condens. Matter **3**, 3285 (1991).